Acta Crystallographica Section D
Biological Crystallography
ISSN 0907-4449

Structure of an acidic phospholipase A_2 from Indian saw-scaled viper (*Echis carinatus*) at 2.6 Å resolution reveals a novel intermolecular interaction

Jayasankar Jasti, M. Paramasivam, A. Srinivasan and T. P. Singh*

Department of Biophysics, All India Institute of Medical Sciences, New Delhi 110 029, India

Correspondence e-mail: tps@aiims.aiims.ac.in

Received 15 July 2003
Accepted 6 October 2003

PDB Reference: phospholipase A_2, 1oz6.

The crystal structure of an acidic phospholipase A_2 from the venom of *Echis carinatus* (saw-scaled viper; $scPLA_2$) has been determined at 2.6 Å resolution and refined to a crystallographic *R* factor of 0.192. Although the overall structure of $scPLA_2$ is essentially similar to those of other group II acidic PLA_2s from different species, it shows unique features in several parts. Particularly noteworthy is the C-terminal part, which folds differently to those of other group II PLA_2s. This part is considered to be responsible for inhibition of the platelet-aggregation activity. The calcium-binding loop is tightly organized with sevenfold coordination. Another striking feature of $scPLA_2$ is the involvement of Asn79 $O^{\delta1}$ of a symmetry-related molecule in a coordination linkage with Ca^{2+} of the calcium-binding loop. This is the first observation of an internal metal ion participating in an intermolecular interaction. The β-wing of a molecule is deeply inserted into the hydrophobic channel of another molecule and forms several intermolecular interactions. This results in the formation of an infinite chain of molecules. These chains are stacked in an antiparallel arrangement in the crystals.

1. Introduction

Phospholipase A_2 (PLA_2; EC 3.1.1.4) is involved in the formation of fatty acids and lysophospholipids by hydrolyzing the 2-acyl ester bond of 1,2-diacyl-3-*sn*-phosphoglycerides (van Deenen & de Haas, 1963). Secretory PLA_2s are low-molecular-weight (~14 kDa) enzymes containing 6–8 disulfide bridges. In addition to their enzymatic function, venom PLA_2s possess a wide variety of pharmacological activities such as neurotoxicity, myotoxicity, initiation and/or inhibition of platelet aggregation, haemolytic, anticoagulant, convulsant, hypotensive, cardiotoxic and oedema-inducing effects (Kini & Evans, 1989). An individual PLA_2 can exhibit one or more of these effects. In order to correlate these properties with structural features, the structures of PLA_2s exhibiting different properties need to be elucidated. To date, the structures of venom PLA_2s from group II which have been analyzed are those from *Vipera russelli* ($vrPLA_2$; Carredano *et al.*, 1998), *Daboia russelli* ($drPLA_2$; Chandra *et al.*, 2000), *V. ammodytes* (vipoxin; Perbandt *et al.*, 1997), *Agkistrodon halys pallas* ($ahPLA_2$; Wang *et al.*, 1996; Zhao *et al.*, 1998; Tang *et al.*, 1998), *A. piscivorous piscivorous* ($apPLA_2$; Holland *et al.*, 1990; Han *et al.*, 1997), *Deinagkistrodon acutus* ($daPLA_2$; Gu *et al.*, 2002), *Bothrops asper* ($baPLA_2$; Ward *et al.*, 1998), *B. pirajai* ($bpPLA_2$; de Azevedo *et al.*, 1998; Lee *et al.*, 2001; Rigden *et al.*, 2003), *B. godmani* ($bgPLA_2$; Arni *et al.*, 1999) and *Crotalus atrox* ($caPLA_2$; Keith *et al.*, 1981). According to their isoelectric points, the group II PLA_2s have been divided into acidic, neutral and basic PLA_2s. They differ broadly in

Table 1
Crystallographic data and refinement statistics.

Values in parentheses are for the last resolution shell.

Space group	$P2_12_12$
Unit-cell parameters (Å)	
a	64.0
b	57.9
c	33.7
Resolution range (Å)	20.0–2.6 (2.65–2.60)
No. unique reflections	3375
Completeness (%)	97 (91)
R_{sym} (%)	9.8 (23.0)
$I/\sigma(I)$	11.2 (2.3)
R factor/R_{free} (%)	19.2/25.7
Protein atoms	951 (B_{avg} = 29.1 Å^2)
Calcium ion	1 (B_{avg} = 18.7 Å^2)
Water molecules	90 (B_{avg} = 38.8 Å^2)
R.m.s. deviations	
B factor, main-chain residues (Å^2)	1.1
B factor, side-chain residues (Å^2)	2.0
Bond lengths† (Å)	0.015
Bond angles† (Å)	2.2
Residues in allowed regions (%)	86
Residues in additionally allowed regions (%)	14
Overall average G factor‡	0.16

† Target stereochemistry from Engh & Huber (1991). ‡ G factor as reported by *PROCHECK* (Laskowski *et al.*, 1993).

enzymatic activity, lethal potency and pharmacological effects (Chen *et al.*, 1987; Kondo *et al.*, 1989). So far, crystal structures of only three acidic PLA_2s, those from *A. halys pallas* (Wang *et al.*, 1996), *A. halys blomhoffii* (Tomoo *et al.*, 1992; structure coordinates not available) and *Deinagkistrodon acutus* (Gu *et al.*, 2002), have been reported.

The acidic PLA_2 from Indian saw-scaled viper (*Echis carinatus*; scPLA2) belongs to group II and exhibits strong platelet-aggregation inhibition and induces oedema (Kemparaju *et al.*, 1999). However, the structural details associated with these effects are not yet known. Here, we report the cDNA sequence and crystal structure of $scPLA_2$ at 2.6 Å resolution. This is the first PLA_2 structure from the saw-scaled viper. The structure reveals a novel intermolecular interaction between the hydrophobic channel of a molecule and the β-wing of a symmetry-related molecule.

2. Materials and methods

2.1. Sequence determination

Tissues from the venom glands of the saw-scaled viper were obtained from the Irula snake farm with the permission of the Government of Tamil Nadu, India. The isolation of poly-A+ mRNA and cDNA synthesis were performed following the manufacturer's protocols (Pharmacia). The conserved nucleotide sequences from PLA_2s of the viper subgroup were used for the design of primers. PCR was performed with Taq polymerase (Promega, USA) using a thermal cycler (MJ Research model PTC-100). The nucleotide sequencing was determined using the cloned double-stranded DNA (pGEM-T) with an automatic sequencer (model ABI-377). Both strands were used for sequencing.

2.2. Purification of PLA_2

Lyophilized *E. carinatus* venom was obtained from Irula cooperative snake farm, Tamil Nadu, India and $scPLA_2$ was purified by two-step affinity and anion-exchange chromatography. 250 mg of crude venom was dissolved in 50 m*M* ammonium acetate buffer pH 6.0 to a concentration of 25 mg ml^{-1}. This was centrifuged at 10 000*g* for 20 min to remove insoluble matter. The supernatant was loaded onto a Cibacron blue F3GA (Pharmacia) column (15 × 2.5 cm), which was pre-equilibrated with 50 m*M* ammonium acetate pH 6.0 at 293 K. The column was washed with the same buffer to remove unbound proteins. It was then eluted stepwise with 50 m*M* ammonium bicarbonate pH 8.5 and with 50 m*M* ammonium carbonate pH 10.5 to obtain $scPLA_2$. The active $scPLA_2$ fractions were pooled and dialyzed against 20 m*M* phosphate buffer pH 6.5 and loaded onto a UNO-Q6 (Pharmacia) anion-exchange column (6 × 2.0 cm), which was pre-equilibrated with 20 m*M* phosphate buffer pH 6.5. It was eluted with a linear gradient of 0.0–0.3 *M* NaCl in 20 m*M* phosphate buffer pH 6.5. The seventh peak in the final elution profile was confirmed to be $scPLA_2$ by SDS–PAGE and by determining the N-terminal amino-acid sequence.

2.3. Crystallization

Lyophilized $scPLA_2$ was dissolved in acetate buffer (50 m*M* sodium acetate, 5 m*M* $CaCl_2$ pH 4.5) to a final concentration of 15 mg ml^{-1}. Crystals of $scPLA_2$ were obtained using the hanging-drop vapour-diffusion method with ethanol as the precipitant. 5 µl of protein solution was mixed with an equal amount of the reservoir solution and equilibrated against 1.0 ml of reservoir solution consisting of 50% ethanol in 5 m*M* $CaCl_2$, 50 m*M* sodium acetate pH 4.5. Thin needle-shaped crystals of dimensions 0.1 × 0.05 × 0.05 mm appeared within 72 h.

2.4. X-ray intensity data collection and processing

The X-ray intensity data were collected at 283 K using a MAR 345dtb image-plate scanner mounted on a Rigaku RU-300 rotating-anode X-ray generator. The crystals diffracted to 2.6 Å. The data were processed and scaled with *DENZO* and *SCALEPACK* (Otwinowski & Minor, 1997), respectively. The crystals belong to the orthorhombic space group $P2_12_12$, with one molecule in the asymmetric unit. The results of the data-collection and processing statistics are given in Table 1.

2.5. Structure determination and refinement

The structure was determined by molecular replacement using *MOLREP* v.7.3 (Vagin & Teplyakov, 1997) from the *CCP*4 v.4.2 software suite (Collaborative Computational Project, Number 4, 1994) using the coordinates of PLA_2 from *Daboia russelli pulchella* (PDB code 1fb2) as the search model. The rotation and translation functions calculated with data in the resolution range 12.0–4.0 Å yielded a clear solution with a correlation coefficient of 41.7 (28.9) and an R factor of

51.8% (56.7) (values in parentheses are for the first noise peak). The stacking arrangement of the molecules in the unit cell for this solution yielded no unfavourable intermolecular contacts.

The output coordinates from *MOLREP* were subjected to 20 cycles of rigid-body refinement and then to restrained refinement with *REFMAC*5 (Murshudov *et al.*, 1999). This reduced the R factor to 30.5% with an $R_{\rm free}$ of 45.6% (5% of the reflections were used to calculate $R_{\rm free}$ and were not included in the refinement). Model building into $(2F_o - F_c)$ Fourier and $(F_o - F_c)$ difference Fourier maps was performed using the program *O* (Jones *et al.*, 1991) on a Silicon Graphics O2 workstation. The refinement was also performed with *CNS* v.1.1 (Brünger *et al.*, 1998) with several cycles of rigid-body, simulated-annealing, positional and *B*-factor protocols interspersed with manual rebuilding. This further decreased the R and $R_{\rm free}$ factors to 26.5 and 34.1%, respectively. The difference Fourier $(F_o - F_c)$ map at 8σ cutoff clearly indicated the presence of a calcium ion at the centre of the calcium-binding loop. Water molecules were added using *ARPP*/*REFMAC* (Perrakis *et al.*, 1999) until there was no further decrease in $R_{\rm free}$ and were manually checked and adjusted for good hydrogen-bonding geometry with the model using the program *O* (Jones *et al.*, 1991).

```
5'  T AGG GCG AAT TGG GCC CGA CGT CGC ATG CTC CCG GCC GCC ATG GCG GCC GCG GGA  55

      ATT CGA TTC GGA GGC GAT TAA CGG GGT CTG CTC ATT TCC AGG TCT GGA TTC AGG 109

      AGG ATG AAG ACT CTC TGG ATA GTG GCC GTG TGG CTG ATC GCC GTC GAA GGA AAC 163
  -16     Met Lys Thr Leu Trp Ile Val Ala Val Trp Leu Ile Ala Val Glu Gly Asn   1

      CTT TAC CAA TTC GGA AGG ATG ATC TGG AAT AGG ACG GGG AAA CTA CCT ATA CTC 217
      Leu Tyr Gln Phe Gly Arg Met Ile Trp Asn Arg Thr Gly Lys Leu Pro Ile Leu  19

      TCC TAC GGC TCT TAT GGA TGC TAC TGT GGC TGG GGG GGC CAA GGC CCG CCA AAG 271
      Ser Tyr Gly Ser Tyr Gly Cys Tyr Cys Gly Trp Gly Gly Gln Gly Pro Pro Lys  37

      GAC GCC ACT GAC CGC TGC TGC TTG GTG CAC GAC TGC TGT TAC ACA AGA GTG GGT 325
      Asp Ala Thr Asp Arg Cys Cys Leu Val His Asp Cys Cys Tyr Thr Arg Val Gly  55

      GAC TGT AGC CCC AAA ATG ACC CTC TAC TCC TAC CGC TTT GAA AAC GGG GAT ATC 379
      Asp Cys Ser Pro Lys Met Thr Leu Tyr Ser Tyr Arg Phe Glu Asn Gly Asp Ile  73

      ATC TGC GAT AAC AAA GAC CCG TGC AAG AGG GCA GTT TGT GAG TGT GAC AGG GAG 433
      Ile Cys Asp Asn Lys Asp Pro Cys Lys Arg Ala Val Cys Glu Cys Asp Arg Glu  91

      GCG GCA ATC TGC CTT GGA GAG AAT GTG AAT ACT TAC GAT AAA AAA TAT AAA TCC 487
      Ala Ala Ile Cys Leu Gly Glu Asn Val Asn Thr Tyr Asp Lys Lys Tyr Lys Ser 109

      TAC GAA GAC TGC ACA GAG GAG GTA CAG GAA TGC TAA GTC TCT GCA GGA AGG GAA 541
      Tyr Glu Asp Cys Thr Glu Glu Val Gln Glu Cys ***                         120

      AAA CCC GTC TAA TTA CAC AGT TGT GGT TGT GTT ACT CTA TTA TTC TGA ATG AAT 595

      CAC TAG TGA ATT CGC GGC CG 3'                                          615
```

Figure 1
Nucleotide and deduced amino-acid sequence of saw-scaled viper PLA_2. The arrow indicates the amino-terminus of the mature protein. The stop codon is indicated by ***. The cDNA sequence was deposited in GenBank with accession code AY268946.

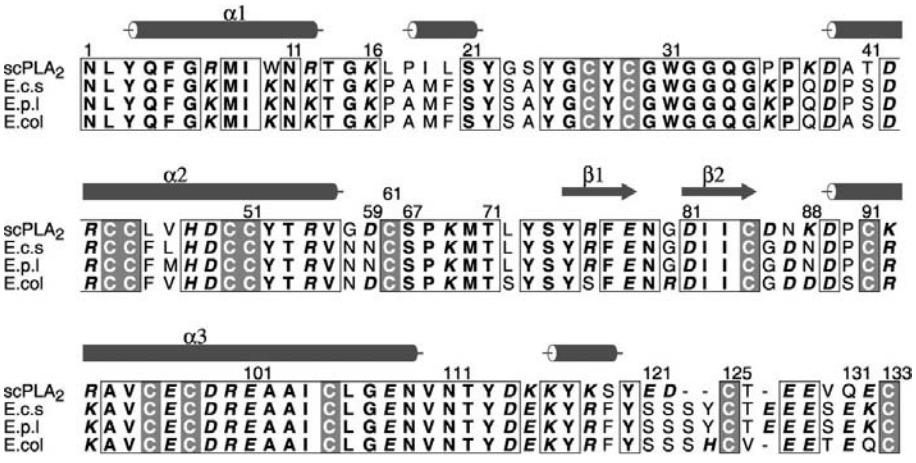

Figure 2
Structure-based sequence alignment of $scPLA_2$ with other *Echis* subgroup PLA_2s. $scPLA_2$, *E. carinatus*; E.c.s, *E. carinatus sochureki*; E.p.l, *E. pyramidum leakeyi*; E.col, *E. coloratus*. Identical residues are boxed. Cys residues are shown in grey. The figure was produced using the program *ALSCRIPT* (Barton, 1993).

3. Results and discussion

3.1. Sequence of $scPLA_2$

The cDNA of $scPLA_2$ reported here is 615 base pairs (bp) in length. It is comprised of 112 nucleotides from the 5′-UTR and an open reading frame of 408 nucleotides encoding 136 amino-acid residues. The signal peptide is 16 amino acids long. There are 95 nucleotides in the 3′-UTR region including the stop codon. The nucleotide and derived amino-acid sequences are given in Fig. 1.

The acidic PLA_2 from saw-scaled viper has a sequence identity of 35–45% with group I PLA_2s, while it shows a sequence identity of 45–65% with the group II PLA_2s to which it belongs. It shows a high sequence identity of 72–74% with PLA_2s of the *Echis* subgroup (*E. carinatus sochureki*, *E. pyramidum leakeyi* and *E. coloratus*; Fig. 2). It may be noted that this is the first crystal structure of a member of the *Echis* subgroup.

3.2. Quality of the model

The final model consists of one molecule of PLA_2 in the asymmetric unit, one calcium ion and 90 water molecules. The model has a good geometry and all the residues fitted well into the electron density. Refinement of the final model converged to an R factor of 19.2% and an $R_{\rm free}$ of 25.7% for 3375 unique reflections in the resolution range 20.0–2.6 Å. In the Ramachandran plot (Ramachandran & Sasisekharan, 1968), 86% of the residues were in the

most favoured regions, while no residues were found in the disallowed regions (Table 1).

3.3. Overall structure of scPLA$_2$

The structure of scPLA$_2$ displays all the characteristics of group II PLA$_2$s, with three long α-helices (Tyr3–Arg12, Asp39–Val55 and Asp89–Asn109), one double-stranded antiparallel β-sheet (Tyr75–Glu78 and Asp81–Cys84) designated as β-wing and a calcium-binding loop (Tyr25–Gly35) (Fig. 3). These structural elements as well as the C-terminal ridge (residues 127–133; unique to group II PLA$_2$s) are cross-linked by seven disulfide bonds. The structures of the active site and the hydrophobic channel are also highly conserved. Least-squares superpositions of the C$^\alpha$ atoms of scPLA$_2$ on the equivalent C$^\alpha$ atoms of the venom group I and II PLA$_2$s show r.m.s. deviations of 0.9–1.2 and 0.8–1.1 Å respectively. This suggests that the overall folding of the scPLA$_2$ chain shows nearly identical variations with both groups of PLA$_2$s.

3.4. Calcium-binding loop

Calcium is an essential cofactor for the catalytic activity of the enzyme. The calcium ion binds at the highly conserved calcium-binding loop and the ligand O atoms form a distorted pentagonal bipyramidal structure. The calcium ion in the calcium-binding loop is coordinated to Tyr28 O (Ca$^{2+}\cdots$O = 2.49 Å), Gly30 O (Ca$^{2+}\cdots$O = 2.66 Å), Gly32 O (Ca$^{2+}\cdots$O = 2.55 Å), Asp49 O$^{\delta1}$ (Ca$^{2+}\cdots$O$^{\delta1}$ = 2.93 Å), Asp49 O$^{\delta2}$ (Ca$^{2+}\cdots$O$^{\delta2}$ = 2.71 Å), Ow90 (Ca$^{2+}\cdots$Ow90 = 2.35 Å) and to the symmetry-related Asn79 O$^{\delta1}$ (Ca$^{2+}\cdots$O$^{\delta1}$ = 2.86 Å). The symmetry-related Asn79 O$^{\delta1}$ has replaced one of the two conserved water molecules that are coordinated to the calcium ion in other calcium-containing PLA$_2$s (Fig. 4). This is the first observation of the calcium ion of the calcium-binding loop being coordinated by a symmetry-related protein atom.

3.5. Hydrophobic channel

PLA$_2$ binds and catalyzes the hydrolysis of water-insoluble phospholipids with the aid of a unique hydrophobic channel. The hydrophobic channel supports the access of hydrophobic phospholipids to the polar active-site residues where catalysis occurs. Leu2, Tyr3, Phe5 and Gly6 form the lower side of the hydrophobic channel, while Trp10, Leu17, Pro18, Ile19, Leu20, Tyr22 and Leu106 form the upper wall of the channel. Ile9, Ala102 and Ala103 form the base of the channel. Adjacent to these hydrophobic residues, a series of polar residues, Arg7, Asn11, Thr13 and Lys69, play a significant role in PLA$_2$ function. When PLA$_2$ binds to a membrane, the polar residues at the entrance of the channel may help in the desolvation of the polar head groups of the substrate and facilitate its entry through the hydrophobic channel (Zhou & Schulten, 1996).

3.6. Molecular association and crystal packing

scPLA$_2$ exists as a monomer in the crystalline state (hereafter referred to as molecule *A*). It forms a unique molecular association with one of the symmetry-related molecules in the crystals (hereafter referred to as molecule *B*). The β-wing of molecule *B* is inserted deeply into the hydrophobic channel of molecule *A* like an arrow (Fig. 5*a*). The residues of the β-wing of molecule *B* interact strongly with those of the calcium-binding loop, including the calcium ion, of molecule *A* (Fig. 5*b*). In addition to the coordination linkage between Asn79 O$^{\delta1}$ and Ca^{2+}, the side chain of Lys69 of molecule *A* forms a salt bridge with the side chain of Asp81 of molecule *B*.

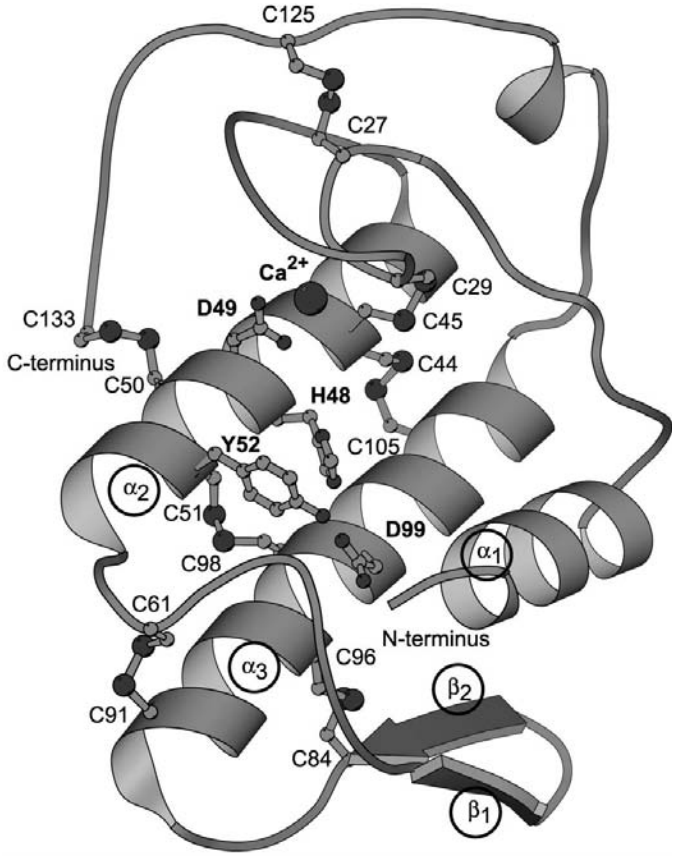

Figure 3
Overall structure of scPLA$_2$. The active-site residues and the conserved cysteine residues are represented in ball-and-stick representation. The figure was produced using the program *MOLSCRIPT* (Kraulis, 1991).

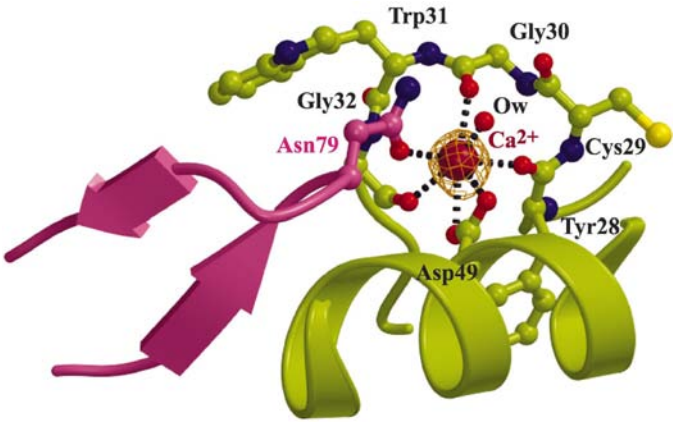

Figure 4
Interaction of Ca^{2+} in the calcium-binding loop. The difference Fourier ($F_o - F_c$) map for Ca^{2+} is contoured at 8σ. The symmetry-related Asn79 is shown in pink. The figure was produced using the programs *BOBSCRIPT* (Esnouf, 1997) and *Raster3D* (Merritt & Murphy, 1994).

Table 2
Hydrogen-bond distances (Å) between molecule *A* and symmetry-related molecule *B*.

A	*B*	Distance (Å)
Trp31 $N^{\varepsilon1}$	Glu78 O	3.1
Gly32 N	Asn79 $O^{\delta1}$	3.2
Gly33 N	Glu78 $O^{\varepsilon1}$	3.0
Gln34 $O^{\varepsilon1}$	Arg76 NH1	3.2
	Arg76 NH2	3.0
Arg43 NH1	Leu72 O	3.1
Thr53 O	Asn11 $N^{\delta2}$	2.8
Asp59 N	Asn11 O	3.0
Lys69 N^{ζ}	Asp81 $O^{\delta1}$	2.8
Ca^{2+}	Asn79 $O^{\delta1}$	2.8

There are three hydrogen bonds involving Gly33, Gln34 and Thr53 of molecule *A* and Glu78, Arg76 and Asn11 of molecule *B* (Table 2). Although only small regions of the two molecules are in contact, the nature of these interactions suggests that the two molecules are strongly associated. In spite of such strong intermolecular interactions, the conformation of the β-wing in the present structure does not differ significantly from that observed in other group II PLA_2 structures (Carredano *et al.*, 1998; Chandra *et al.*, 2000; Perbandt *et al.*, 1997; Wang *et al.*, 1996; Gu *et al.*, 2002). Therefore, the basis of the unique behaviour of the β-wing in $scPLA_2$ may be understood from its amino-acid sequence Arg76-Phe77-Glu78-Asn79-Gly80-Asp81. When compared with other group II PLA_2s of known crystal structure (Carredano *et al.*, 1998; Chandra *et al.*, 2000; Perbandt *et al.*, 1997; Wang *et al.*, 1996; Gu *et al.*, 2002), the combination of Arg76, Glu78, Asn79 and Asp81 is unique to $scPLA_2$. The neighbouring acidic residues Glu78 and Asp81 push the central residue Asn79, which sits at the apex of the hairpin loop, towards the calcium ion of the neighbouring molecule to form a coordination linkage. The other two key interactions involve Arg76 and Asp81 of molecule *B* with Gln34 and Lys69 of molecule *A*, respectively. The combination of these interactions is unique and is based on the specific amino-acid sequence of the β-wing in $scPLA_2$ compared with those observed in other group II PLA_2 structures (Carredano *et al.*, 1998; Chandra *et al.*, 2000; Perbandt *et al.*, 1997; Wang *et al.*, 1996; Gu *et al.*, 2002).

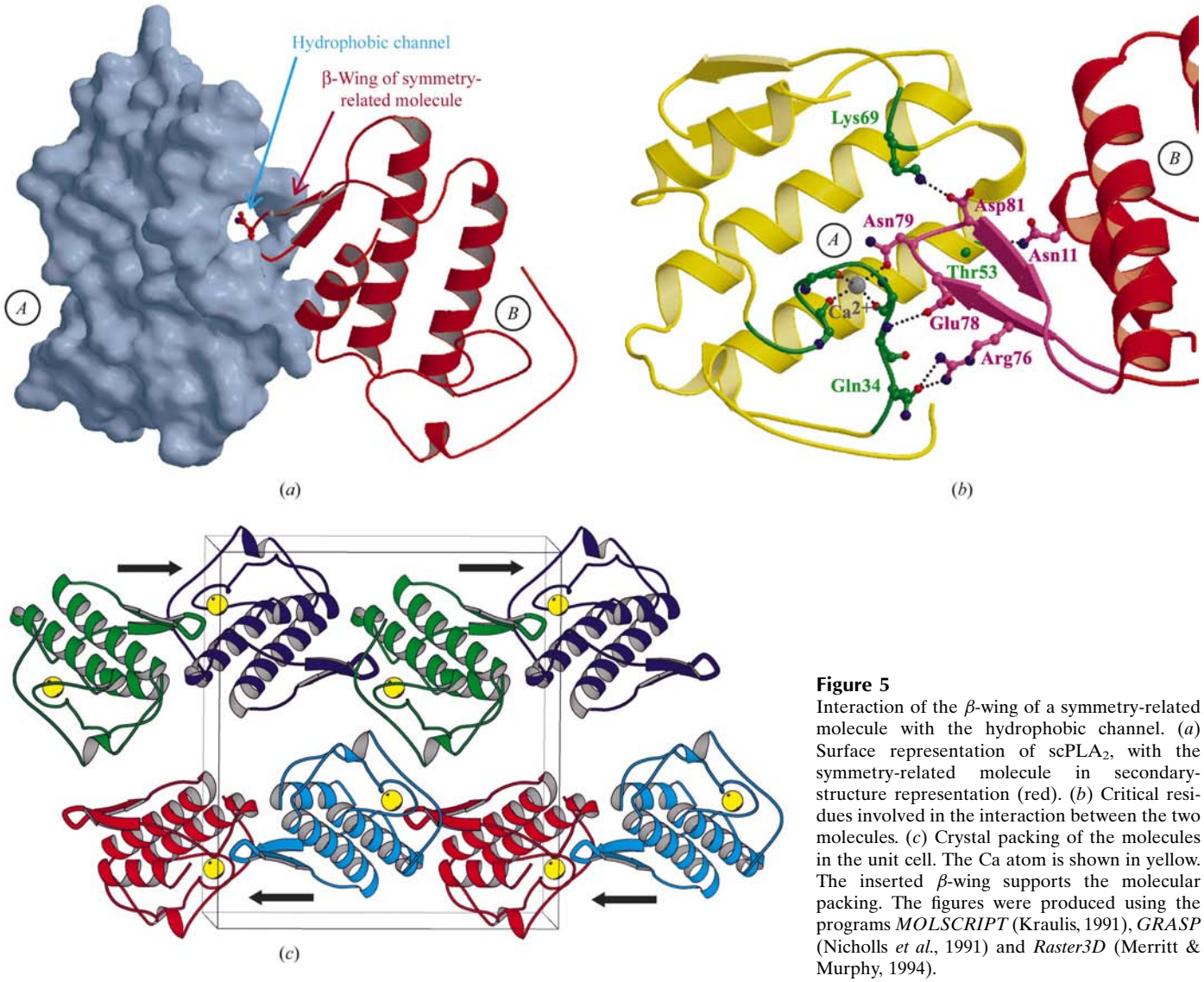

Figure 5
Interaction of the β-wing of a symmetry-related molecule with the hydrophobic channel. (*a*) Surface representation of $scPLA_2$, with the symmetry-related molecule in secondary-structure representation (red). (*b*) Critical residues involved in the interaction between the two molecules. (*c*) Crystal packing of the molecules in the unit cell. The Ca atom is shown in yellow. The inserted β-wing supports the molecular packing. The figures were produced using the programs *MOLSCRIPT* (Kraulis, 1991), *GRASP* (Nicholls *et al.*, 1991) and *Raster3D* (Merritt & Murphy, 1994).

It is a well known fact that the pH, the presence of Ca^{2+} and the concentration of PLA_2 molecules all influence the oligomerization equilibrium of PLA_2s (Myatt *et al.*, 1991). The type of association observed here could not lead to stable dimerization in the physiological state as the association appears to be physically unfavourable, with only the β-wing of molecule *B* interacting with the calcium-binding loop of molecule *A*, while the rest of the molecule hangs in the air (Fig. 5*a*). However, this kind of association may be helpful in maintaining the enzyme in an inactive state in the snake-venom sacs, where it occurs at very high concentrations (Fremont *et al.*, 1993; Segelke *et al.*, 1998). The intermolecular interactions involving the internal calcium ion represent a novel feature of the $scPLA_2$ structure. This may be an important factor in the nucleation of crystal growth and, as observed in the present case, results in the formation of an infinite chain of $scPLA_2$ molecules (Fig. 5*c*). The neighbouring molecular chains are stacked in an antiparallel arrangement and are primarily held together by solvent-mediated interactions. A few direct hydrogen bonds involving residues Gln34, Glu121 and Cys125 from one chain and residues Ser119 and Glu121 from another chain are also observed.

3.6.1. Catalytic activity of $scPLA_2$. The active-site region of scPLA2 consists of four residues: His48, Asp49, Tyr52 and Asp99. The active-site residues belong to two antiparallel helices, α2 and α3. These two helices form the back wall of the substrate-binding surface (Fig. 3). The stereochemical arrangement of the catalytic residues is supported by the formation of hydrogen bonds between them. The side chains of His48, Tyr52 and Asp99 are directly bonded to each other, while the side chain of Asp49 interacts *via* a water molecule with His48. This water molecule is required for catalytic activity.

3.7. Pharmacological sites in $scPLA_2$

It has been indicated that PLA_2s containing a high density of positively charged residues in the stretch from residues 55 to 77 display a strong anticoagulant activity (Kini & Evans, 1989; Carredano *et al.*, 1998; Chandra *et al.*, 2000). For instance, neurotoxic activity is observed in $drPLA_2$, which contains Lys69, Arg72, Lys74 and Arg76 as a stretch of positively charged residues. On the other hand, in $scPLA_2$, Leu at position 72 and Ser at position 74 disrupt the continuity of positively charged residues and thus hamper its neurotoxicity. Also, when the segment 55–77 of $scPLA_2$ was compared with the corresponding segment of $drPLA_2$ it showed an r.m.s. shift of 0.8 Å, indicating an additional slight deviation of the backbone conformations of the two molecules in this region.

Furthermore, in neurotoxic $drPLA_2$, like other neurotoxic PLA_2s, residues 55–61 adopt a well defined type I β-turn conformation with a hydrogen bond between Leu55 O and Cys61 N. The neighbouring loop 85–94 adopts a compact structure, with several intra-loop hydrogen bonds. The two loops are linked by a conserved disulfide bridge and also by a strong electrostatic interaction between Asp59 and Arg94. The non-neurotoxic $scPLA_2$ (Kemparaju *et al.*, 1999), like the other non-neurotoxic PLA_2s from *A. piscivorous piscivorous* (Holland *et al.*, 1990), *V. russelli* (Carredano *et al.*, 1998) and *C. atrox* (Keith *et al.*, 1981), display grossly dissimilar conformations for both the segments (r.m.s. shift of 1.2 Å for equivalent C^{α} atoms): segment 55–61 adopts an extended conformation and loop 85–94 is held rather loosely with limited intra-loop interactions.

3.8. Platelet-aggregation inhibition site

The effect of PLA_2 on platelet aggregation appears to be a specific activity rather than a simple hydrolysis of platelet membrane phospholipids, as not all PLA_2 enzymes affect platelet aggregation, despite their common catalytic activity (Ouyang & Huang, 1984). On the basis of their platelet function, venom PLA_2 enzymes have been broadly divided into three classes. The PLA_2s of class A promote platelet aggregation, while those of class B cause inhibition of platelet aggregation. The enzymes of class B can be further divided into two groups, referred to as B1 and B2 based on their inhibition of platelet-aggregation activity. Group B1 enzymes achieve platelet aggregation based on their enzymatic activity, whereas group B2 PLA_2s produce their effects by a non-enzymatic mechanism. The class C PLA_2s exhibit unique biphasic effects, initiating aggregation at low concentrations and with short incubation times but inhibiting aggregation at high concentrations and with long incubation times (Kini & Evans, 1988).

Platelet aggregation is needed for platelet retraction and wound repair. Interference with platelet aggregation may lead to debilitation or death. As $scPLA_2$ inhibits platelet aggregation independently of its catalytic activity (Kini & Evans, 1990; Kemparaju *et al.*, 1999), it is placed in class B2.

Another important feature of the $scPLA_2$ structure is its C-terminal segment (residues 112–133), which shows significant conformational differences when compared with other group II PLA_2s. The putative anti-platelet site is rich in charged residues, Asp114, Lys115, Lys116, Lys118, Glu121 and Asp122, which are interspersed with three tyrosines, Tyr113, Tyr117 and Tyr120. In addition, the hydrophobic residues Trp10, Leu17, Leu19 and Leu20 provide a unique structural surrounding for the charged residues, making an overall contribution to the anti-platelet site and extending it up to the upper wall of the hydrophobic channel. The superimposition of C^{α} atoms of the segment 112–133 of $scPLA_2$ on the corresponding C^{α} atoms of other venom group II PLA_2s shows r.m.s. deviations in the range 2.5–3.2 Å [$drPLA_2$ (PDB code 1cl5), 2.4 Å; $vrPLA_2$ (1vip), 2.5 Å; $acPLA_2$ (1mc2), 2.5 Å; myotoxin II (1god), 2.6 Å; agkistrodotoxin (1a2a), 2.9 Å; vipoxin (1jlt), 3.2 Å].

In *A. halys pallas* PLA_2, it was reported that Glu6 contributed a charge effect at one end of the hydrophobic patch and was considered to be essential for its anti-platelet effect (Wang *et al.*, 1996; Liu *et al.*, 2001), whereas in $scPLA_2$ residue 6 is Gly and there is no acidic residue at this end of the hydrophobic patch. Also, the continuous hydrophobic patch in $scPLA_2$ is disrupted by Lys118. Thus, it may be considered that

the crucial anti-platelet region in scPLA$_2$ may be around Asp114.

The C-terminal region of scPLA$_2$ makes several interactions with the rest of the molecule. These interactions include Tyr113 OH···Ser21 O (2.5 Å), Asp114 N···Tyr25 OH (3.1 Å), Tyr117 O···Gly26 N (3.0 Å), Cys125 O···Gln34 N$^{\varepsilon2}$ (3.5 Å), Glu128 O···Gly35 N (3.1 Å) and Gln130 N$^{\varepsilon2}$···Gly35 O (3.2 Å). In addition, there are several water-mediated hydrogen bonds and hydrophobic interactions. The presence of two disulfide bridges between the C-terminal region and the rest of the molecule imparts extra stability to this part of the molecule.

4. Conclusions

Phospholipase A$_2$ from Indian saw-scaled viper exists as a monomer. However, a novel molecular association has been observed in its crystals in which the β-wing of a symmetry-related molecule is completely inserted into the hydrophobic channel of another molecule. Ca^{2+} is sevenfold coordinated with three O atoms from the carbonyl groups of the calcium-binding loop, two from the carboxyl group of Asp49, one from a water molecule and the seventh from the side chain of Asn79 of the β-wing of a symmetry-related molecule. This is the first example of an intermolecular coordination of the calcium ion in the calcium-binding loop. In addition to the coordination linkage and a salt bridge between Lys69 and Asp81 (symmetry-related), several hydrogen bonds are also formed between the calcium-binding loop and the β-wing.

Another important feature of the acidic scPLA$_2$ is its role as an inhibitor of platelet-aggregation activity. The amino-acid sequence and conformational characteristics indicate that the site of this activity is situated in the C-terminal part of the molecule. The conformation of the C-terminal region (residues 113–122) of scPLA$_2$ differs strikingly from that of PLA$_2$s that lack the capability to inhibit platelet-aggregation activity. A series of charged residues in this region may be involved in binding to the platelet receptors GPIIb-IIIa, leading to the anti-platelet effects. Further studies using site-directed mutagenesis may also be needed to fully establish the structure–function relationship.

JJ thanks the Council of Scientific and Industrial Research, New Delhi, India for the award of a fellowship.

References

Arni, R. K., Fontes, M. R., Barberato, C., Gutierrez, J. M., Diaz, C. & Ward, R. J. (1999). *Arch. Biochem. Biophys.* **366**, 177–182.

Azevedo, W. F. de Jr, Ward, R. J., Canduri, F., Soares, A., Giglio, J. R. & Arni, R. K. (1998). *Toxicon*, **36**, 1395–1406.

Barton, G. J. (1993). *Protein Eng.* **6**, 37–40.

Brünger, A. T., Adams, P. D., Clore, G. M., Delano, W. L., Gros, P., Grosse-Kunstleve, R. W., Jiang, J.-S., Kuszewski, J., Nilges, N., Pannu, N. S., Read, R. J., Rice, L. M., Simonson, T. & Warren, G. L. (1998). *Acta Cryst.* D**54**, 905–921.

Carredano, E., Westerlund, B., Persson, B., Saarinen, M., Ramaswamy, S., Eaker, D. & Eklund, H. (1998). *Toxicon*, **36**, 75–92.

Chandra, V., Kaur, P., Srinivasan, A. & Singh, T. P. (2000). *J. Mol. Biol.* **296**, 1117–1126.

Chen, Y. C., Maraganore, J. M., Reardon, I. & Heinrikson, R. L. (1987). *Toxicon*, **25**, 401–409.

Collaborative Computational Project, Number 4 (1994). *Acta Cryst.* D**50**, 760–763.

Deenen, L. L. M. van & de Haas, G. H. (1963). *Biochem. Biophys. Acta*, **70**, 538–553.

Engh, R. A. & Huber, R. (1991). *Acta Cryst.* A**47**, 392–400.

Esnouf, R. M. (1997). *J. Mol. Graph.* **15**, 132–134.

Fremont, D. H., Anderson, D. H., Wilson, I. A., Dennis, E. A. & Xuong, N. H. (1993). *Proc. Natl Acad. Sci. USA*, **90**, 342–346.

Gu, L., Zhang, H., Song, S., Zhou, Y. & Lin, Z. (2002). *Acta Cryst.* D**58**, 104–110.

Han, S. K., Yoon, E. T., Scott, D. L., Sigler, P. B. & Cho, W. (1997). *J. Biol. Chem.* **272**, 3573–3582.

Holland, D. R., Clancy, L. L., Muchmore, S. W., Ryde, T. J., Einspahr, H. M., Finzel, B. C., Heinrikson, R. L. & Watenpaugh, K. D. (1990). *J. Biol. Chem.* **265**, 17649–17656.

Jones, T. A., Zou, J., Cowan, S. & Kjeldgaard, W. J. M. (1991). *Acta Cryst.* A**47**, 110–119.

Keith, C., Feldman, D. S., Deganello, S., Glick, J., Ward, K. B., Jones, E. O. & Sigler, P. B. (1981). *J. Biol. Chem.* **256**, 8602–8607.

Kemparaju, K., Krishnakanth, T. P. & Veerabasappa Gowda, T. (1999). *Toxicon*, **37**, 1659–1671.

Kini, R. M. & Evans, H. J. (1988). *Thromb. Haemost.* **60**, 170–173.

Kini, R. M. & Evans, H. J. (1989). *Toxicon*, **27**, 613–635.

Kini, R. M. & Evans, H. J. (1990). *Toxicon*, **28**, 1387–1422.

Kondo, K., Zhang, J., Xu, K. & Kagamiyama, H. (1989). *J. Biochem. (Tokyo)*, **105**, 196–203.

Kraulis, P. J. (1991). *J. Appl. Cryst.* **24**, 946–950.

Laskowski, R. A., MacArthur, M. W., Moss, D. S. & Thornton, J. M. (1993). *J. Appl. Cryst.* **26**, 283–291.

Lee, W. H., da Silva Giotto, M. T., Marangoni, S., Toyama, M. H., Polikarpov, I. & Garratt, R. C. (2001). *Biochemistry*, **40**, 28–36.

Liu, X., Wu, X. & Zhou, Y. (2001). *J. Nat. Toxins*, **10**, 43–55.

Merritt, E. A. & Murphy, M. E. P. (1994). *Acta Cryst.* D**50**, 869–873.

Murshudov, G. N., Vagin, A. A., Lebedev, A., Wilson, K. S. & Dodson, E. J. (1999). *Acta Cryst.* D**55**, 247–255.

Myatt, E. A., Stevens, F. J. & Sigler, P. B. (1991). *J. Biol. Chem.* **266**, 16331–16335.

Nicholls, A., Sharp, K. A. & Honig, B. (1991). *Proteins*, **11**, 281–296.

Otwinowski, Z. & Minor, W. (1997). *Methods Enzymol.* **276**, 307–326.

Ouyang, C. & Huang, T. F. (1984). *Toxicon*, **22**, 705–718.

Perbandt, M., Wilson, J. C., Eschenburg, S., Mancheva, I., Aleksiev, B., Genov, N., Willingmann, P., Weber, W., Singh, T. P. & Betzel, C. (1997). *FEBS Lett.* **412**, 573–577.

Perrakis, A., Morris, R. J. & Lamzin, V. S. (1999). *Nature Struct. Biol.* **6**, 458–463.

Ramachandran, G. N. & Sasisekharan, V. (1968). *Adv. Protein Chem.* **23**, 283–438.

Rigden, D. J., Hwa, L. W., Marangoni, S., Toyama, M. H. & Polikarpov, I. (2003). *Acta Cryst.* D**59**, 255–262.

Segelke, B. W., Nguyen, D., Chee, R., Xuong, N. H. & Dennis, E. A. (1998). *J. Mol. Biol.* **279**, 223–232.

Tang, L., Zhou, Y. C. & Lin, Z. J. (1998). *J. Mol. Biol.* **282**, 1–11.

Tomoo, K., Ohishi, H., Doi, M., Ishida, T., Inoue, M., Ikeda, K., Hata, Y. & Samejima, Y. (1992). *Biochem. Biophys. Res. Commun.* **184**, 137–143.

Vagin, A. & Teplyakov, A. (1997). *J. Appl. Cryst.* **30**, 1022–1025.

Wang, X. Q., Yang, J., Gui, L. L., Lin, Z. J., Chen, Y. C. & Zhou, Y. C. (1996). *J. Mol. Biol.* **255**, 669–676.

Ward, R. J., de Azevedo, W. F. Jr & Arni, R. K. (1998). *Toxicon*, **36**, 1623–1633.

Zhao, K., Song, S., Lin, Z. & Zhou, Y. (1998). *Acta Cryst.* D**54**, 510–521.

Zhou, F. & Schulten, K. (1996). *Proteins*, **25**, 12–27.